

Analysis of ultra-high sensitivity configuration in chip-integrated photonic crystal microcavity bio-sensors

Swapnajit Chakravarty, Amir Hosseini, Xiaochuan Xu, Liang Zhu, Yi Zou, and Ray T. Chen

Citation: [Applied Physics Letters](#) **104**, 191109 (2014); doi: 10.1063/1.4875903

View online: <http://dx.doi.org/10.1063/1.4875903>

View Table of Contents: <http://scitation.aip.org/content/aip/journal/apl/104/19?ver=pdfcov>

Published by the [AIP Publishing](#)

Articles you may be interested in

[Highly sensitive bovine serum albumin biosensor based on liquid crystal](#)

Appl. Phys. Lett. **104**, 043705 (2014); 10.1063/1.4863740

[Planar lens integrated capillary action microfluidic immunoassay device for the optical detection of troponin I](#)

Biomechanics **7**, 064112 (2013); 10.1063/1.4837755

[Noise analysis and sensitivity enhancement in immunomagnetic nanomechanical biosensors](#)

Appl. Phys. Lett. **93**, 103902 (2008); 10.1063/1.2980036

[Integrated cantilever sensors with a torsional resonance mode for ultrasensitive on-the-spot bio/chemical detection](#)

Appl. Phys. Lett. **90**, 041901 (2007); 10.1063/1.2433753

[Nanoporous leaky waveguide based chemical and biological sensors with broadband spectroscopy](#)

Appl. Phys. Lett. **90**, 011102 (2007); 10.1063/1.2424643

The advertisement features the Lake Shore CRYOTRONICS logo on the left, which includes a stylized blue and white square icon. In the center, there is a photograph of the Model 8501 THz System, showing a computer monitor displaying a graph, a keyboard, and a large, dark, cylindrical cryogenic chamber with various sensors and cables attached. To the right of the image, the text reads 'Model 8501 THz System' in a large, bold, blue font, followed by 'A new integrated solution for non-contact characterization' in a smaller, black font. The background of the advertisement is a dark blue gradient with a white line graph overlay.

Analysis of ultra-high sensitivity configuration in chip-integrated photonic crystal microcavity bio-sensors

Swapnajt Chakravarty,^{1,a)} Amir Hosseini,¹ Xiaochuan Xu,¹ Liang Zhu,² Yi Zou,² and Ray T. Chen^{1,2,b)}

¹Omega Optics, Inc., Austin, Texas 78757, USA

²Department of Electrical and Computer Engineering, University of Texas at Austin, Austin, Texas 78758, USA

(Received 13 March 2014; accepted 24 April 2014; published online 14 May 2014)

We analyze the contributions of quality factor, fill fraction, and group index of chip-integrated resonance microcavity devices, to the detection limit for bulk chemical sensing and the minimum detectable biomolecule concentration in biosensing. We analyze the contributions from analyte absorbance, as well as from temperature and spectral noise. Slow light in two-dimensional photonic crystals provide opportunities for significant reduction of the detection limit below 1×10^{-7} RIU (refractive index unit) which can enable highly sensitive sensors in diverse application areas. We demonstrate experimentally detected concentration of 1 fM (67 fg/ml) for the binding between biotin and avidin, the lowest reported till date. © 2014 AIP Publishing LLC. [<http://dx.doi.org/10.1063/1.4875903>]

In recent years, various integrated optical devices have been developed for label-free bio-sensing such as ring resonators,¹ wire waveguides,² surface plasmon resonance (SPR),³ and photonic crystal (PC) microcavities.⁴⁻⁶ The detection principle is based on a change in the refractive index, and hence the transduced signal caused by the specific binding of the biomolecule of interest to its specific conjugate biomolecule receptor bound to the optical device substrate. The device sensitivity is determined by the magnitude of light-matter interaction.

For early bio-pathogen detection, a sensor with highest sensitivity is desired. The sensitivity is measured by the magnitude of the resonance wavelength shift for a fixed concentration, as well as the minimum concentration that can be detected. Initial PC designs focused on donor defect modes such as in a L4 microcavity (4 missing holes)⁷ or acceptor defect modes⁸ as in H1 defect cavities, in a triangular lattice of air holes. Later, designs increased the analyte overlap with cavity modes, also referred as fill fraction, for enhanced sensitivity.⁹ Recently, we showed that an increased cavity length results in an increase in the quality factor (Q-factor) of the resonance mode¹⁰⁻¹² that allows smaller changes in concentration to be distinguished. The high Q enhances the interaction time between the optical mode and the analyte while the larger mode volume results in larger fill fraction, both factors resulting in higher sensitivity. We demonstrated experimentally in our side-coupled two-dimensional (2D) PC cavity-waveguide architecture that the magnitude of the slow-down factor in the coupling waveguide contributes to enhanced light-matter interaction.¹¹ Over successive generations, we demonstrated experimentally 50 fM (3.35 pg/ml) sensitivity to the detection of the specific binding of avidin to biotin¹² with a L55 type PC microcavity (55 missing holes).

A question still remains about the relative merits of Q-factor, fill fraction, and group index, when considered in conjunction with different sources of noise in measurements, in order to achieve low detection limits in chip-integrated photonic sensors. While an increased modal overlap with the analyte lowers the detection limit (DL) in an ambient with low absorbance, in water based media such as biological buffers, the DL is significantly influenced by the strong absorbance of water ($\sim 800 \text{ m}^{-1}$) at 1550 nm.¹³ Spectral noise and temperature stabilization noise effects also need to be considered. An optimized design thus needs to balance the resonant device properties versus the various sources of noise in measurements in both bulk chemical sensing and surface biosensing. In this paper, we analyze the relative contributions from various factors to the sensitivity and detection limit. We consider these design aspects to demonstrate experimentally the highest biosensing sensitivity to date in silicon photonic resonator devices in SOI.

Resonator based sensors are characterized by a resonance that shifts in frequency or wavelength in response to a change in the ambient refractive index (for bulk sensing) or a change in the refractive index caused by biomolecules in the vicinity of the surface of the resonator (for biosensing). The response can be understood by first order perturbation theory,¹⁴ in which the change in eigenfrequency $\Delta\omega_m$ of the m th mode can be described as

$$\Delta\omega_m = \frac{\omega_m}{2} \frac{\langle \vec{E}_m | \epsilon_l | \vec{E}_m \rangle_{V_{\text{liquid}}}}{\langle \vec{E}_m | \epsilon_l | \vec{E}_m \rangle_{V_{\text{liquid+dielectric}}}} \frac{\Delta\epsilon_l}{\epsilon_l} \frac{1}{v_{g,m}}, \quad (1)$$

where $\Delta\epsilon_l$ is the change in dielectric constant of the analyte from ϵ_l upon perturbation, and $v_{g,m}$ is the group velocity of the m th mode at the frequency ω_m . Equation (1) implies that the magnitude of wavelength/frequency shift for a given mode caused by a small index change is directly proportional to the fill fraction f_B , defined as the ratio of electric field energy existing outside of a dielectric structure to the total and inversely proportional to the group velocity

^{a)}Author to whom correspondence should be addressed. Electronic mail: swapnajt.chakravarty@omegaoptics.com

^{b)}raychen@uts.cc.utexas.edu

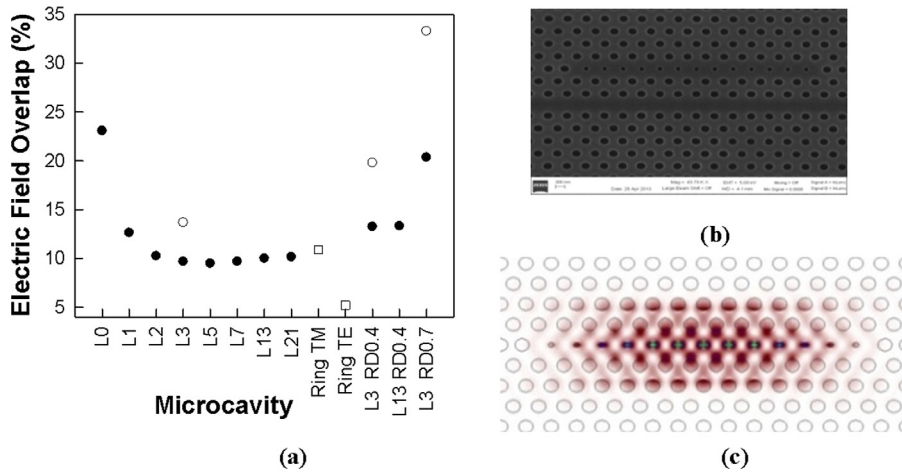


FIG. 1. (a) 2D FDTD simulated fill fraction/field overlap computed for different PC microcavities with $R = 0.275a$ (filled circles), $R = 0.35a$ (open circles), and ring resonator (open square). Ring TM value is taken from Ref. 1 for a ring resonator with diameter of $30 \mu\text{m}$ and width of 500 nm . (b) SEM image of L13 PC microcavity with defect holes (c) mode profile of the confined defect mode in (b).

$$f_B = \frac{\langle \vec{E}_m | \epsilon_l | \vec{E}_m \rangle_{V_{\text{liquid}}}}{\langle \vec{E}_m | \epsilon_l | \vec{E}_m \rangle_{V_{\text{liquid+dielectric}}}}. \quad (2)$$

In Fig. 1(a), the electric field intensity is simulated by 2D finite difference time domain (FDTD) method for different isolated L_i -type PC microcavities ($i =$ number of missing holes) and f_B in water is computed. Typically, in silicon 2D PCs, light is coupled from a PC waveguide (PCW) into an adjacent PC microcavity.^{9–12} An isolated PC microcavity is considered for simulations in order to eliminate the effect of coupling between the PC microcavity and the PCW in cavity-waveguide coupled sensors.^{10–12}

Simulations considered water (refractive index $RI = 1.33$) as the ambient medium and a silicon effective index ($n_{\text{eff}} = 2.9$ for operation at 1550 nm). The radius of the holes of the bulk PC lattice is ($R = 0.275a$, where $a =$ lattice constant). We note from Fig. 1(a) that f_B for the transverse electric (TE) polarized optical mode in water is highest in a L0 cavity (where two adjacent holes in the lattice are shifted by $0.15a$). f_B increases from L3 to L21 PC microcavities. Commercial ring resonator sensors use transverse magnetic (TM) polarization.¹

Defect holes are introduced into the L13 PC microcavity at the antinodes of the resonance mode. A scanning electron micrograph (SEM) of the device is shown in Fig. 1(b). Simulated TE-confined electric intensity profile in Fig. 1(c) shows strong optical localization at the defect holes.

In PC microcavities with defect holes, R_D denotes the radius of the defect hole as a fraction of R . While f_B increases in fractions of percentages from L3 to L21, when

defect holes are introduced, a dramatic increase by 8% in f_B is observed. The resonance mode closest to the PCW transmission band edge is considered.^{10–12} We consider defect holes $>90 \text{ nm}$ diameter for better fabrication tolerance and yield in high volume manufacturing. We refer to such low-index defects as defect holes, rather than nanoholes elsewhere. Such devices have been fabricated by 193 nm immersion lithography.¹⁵

Devices are fabricated on a SOI wafer in 250 nm silicon on a $3 \mu\text{m}$ bottom oxide cladding, which offers better structural stability than free standing membranes. The air hole radius is $R = 108 \text{ nm}$. Fig. 2(a) shows PCW transmission spectrum in water with $R_D = 0.6R$. Defect holes raise the frequency of the resonance mode in the photonic band gap. Consequently, the width of the PCW is reduced for efficient coupling to the PC microcavity at the slow light guiding wavelengths.

The optimized waveguide width indicated in Fig. 2(a) is $W0.855$ where $W0.855$ denotes that the width of the PCW is $0.855 \times \sqrt{3}a$. To determine sensitivity in RIU (refractive index unit), measurements are done in water ($RI = 1.33$) and glycerol ($RI = 1.45$). The bulk sensitivity increased by 66% from $\sim 68 \text{ nm/RIU}$ for L13¹² to $\sim 112 \text{ nm/RIU}$ for the L13 PC microcavity with defect holes for different R_D as shown in Fig. 2(b). The experimentally observed Q is between 1×10^4 and 1.5×10^4 . When $R = 0.35a$, $R_D = 0.7R$, the calculated f_B is 32%; a sensitivity of 200 nm/RIU can thus be expected by linear extrapolation.¹⁶

Equations (1) and (2) clearly indicate that sensitivity of a sensor for bulk sensing can be increased by increasing f_B , so that DL is inversely related to sensitivity (S). However, a

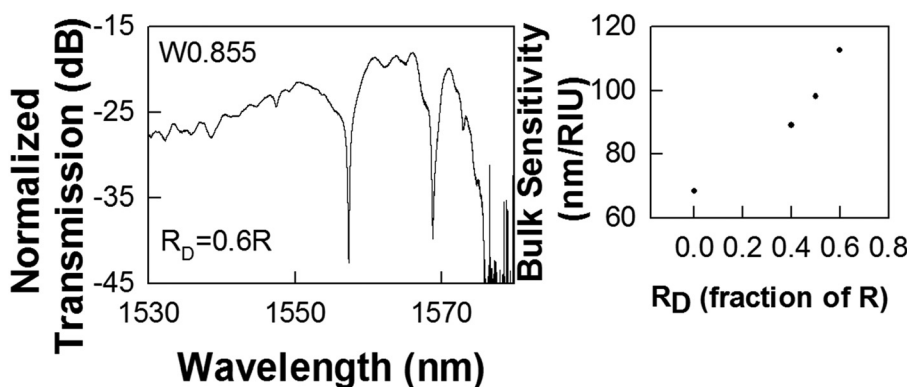


FIG. 2. (a) Transmission spectra for PCWs in water with $R_D = 0.6R$. (b) Bulk sensitivity computed from experimentally observed resonance wavelength shift from water to glycerol for different R_D .

critical parameter in computing DL is the intrinsic quality factor (Q_i) of the resonator and the total Q due to analyte absorbance. In Fig. 3, we estimate the DL for water at $\lambda_m=1550$ nm (absorbance $\alpha \sim 800 \text{ m}^{-1}$). We also consider a hypothetical liquid with $RI = 1.33$ having absorbance of 0.1 m^{-1} at 1550 nm. The total Q is calculated as¹³

$$\frac{1}{Q} = \frac{1}{Q_i} + \frac{1}{Q_\alpha}, \quad (3)$$

$$Q_\alpha = \frac{2\pi n}{\lambda_m f_B \alpha}, \quad (4)$$

where Q_α is the quality factor due to optical absorption at wavelength λ_m , α is the analyte absorbance, and n is the refractive index weighted by f_B . Eight fill fractions (0.01, 0.05, 0.1, 0.2, 0.3, 0.5, 0.75, and 1.0) are considered. n is calculated as $n = f_B n_A + (1 - f_B) n_S$, where n_A and n_S are refractive indices of analyte and dielectric, respectively.

The L_n -type PC cavity can be considered as a closed PCW. Consequently, at the resonance frequency, group index n_g of the mode can be considered the same as in an open ended PC microcavity (or equivalently a PCW). Taking into account the effect of slow light and f_B enhancement on absorbance by a factor γ ,^{14,17} Eq. (4) can now be written as

$$Q_\alpha = \frac{k}{\alpha} = \frac{2\pi n n_{eff}}{\lambda_m f_B \alpha n_g}, \quad (5)$$

$$\gamma = f_B \times \frac{c}{n_{eff}} \times \frac{1}{v_{g,m}}, \quad (6)$$

where k is the wavevector and n_{eff} is the mode effective index with no slow light effect. In a L21 PC microcavity,¹² $n_g \sim 16$. In Figs. 3(a)–3(d), Q is plotted for different Q_i and f_B . In Figs. 3(c) and 3(d), Q is plotted, respectively, for $n_g = 4.3$, a typical value in a ring resonator¹⁸ and for $n_g = 330$ achieved in a PC.¹⁹

Assuming a signal to noise ratio (SNR) of 60 dB, with no other sources of noise, the standard deviation of linewidth ($\Delta\lambda_{FWHM}$) is given by¹³

$$\sigma \approx \frac{\Delta\lambda_{FWHM}}{4.5(SNR^{0.25})}. \quad (7)$$

The DL is calculated as¹³

$$DL = \frac{3\sigma}{S}, \quad (8)$$

where

$$S = \frac{\lambda_m}{n_{eff}} f_B \times n_g. \quad (9)$$

The corresponding DLs are shown in Figs. 3(e)–3(g). At $n_g = 16$ and 1550 nm, while a DL of 3×10^{-10} RIU is achieved at an absorbance of 0.1 m^{-1} for a resonator with $Q = 10^8$ and $f_B = 20\%$, the corresponding DL in water is 1.3×10^{-6} RIU. Figs. 3(i)–3(l) plot the DLs incorporating temperature stabilization (σ) of 10 fm and spectral resolution noise (σ) of 1 pm.¹³ The DL becomes poorer by more than 2 orders of magnitude for the low absorbance hypothetical liquid at $Q_i > 10^5$.

The experimentally observed Q in PC microcavities coupled to PCWs in water¹² at 1550 nm is $\sim 1 \times 10^4$. With $f_B \sim 10\%$, from Eq. (3), $Q_i \sim 1.6 \times 10^4$. Obviously, fabrication induced surface roughness reduces Q , since the designed Q_i in these structures in general is $> 1 \times 10^5$. Still, assuming $Q_i = 1.6 \times 10^4$, at $n_g \sim 16$ for a PC with $f_B = 10\%$, the calculated DL is 3.8×10^{-6} RIU. A typical Q in water for a ring resonator²¹ is 2×10^4 so that calculated Q_i from Eq. (6) is 2.5×10^4 . The corresponding DL is 8×10^{-6} RIU at a typical $f_B = 10\%$. An optimized design in a PC can achieve $f_B > 20\%$ so that achievable DLs (2.6×10^{-6} RIU at $f_B = 20\%$) are better than 2×10^{-5} RIU that will be observed in a

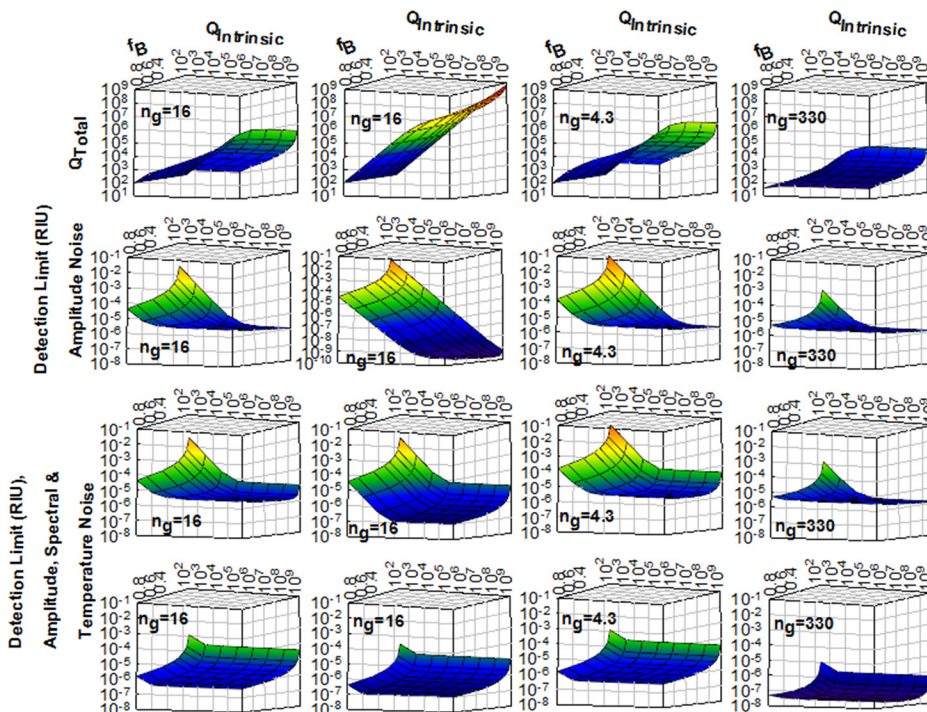


FIG. 3. Effective Q ((a), (c), and (d)) in water with absorbance of 800 m^{-1} and (b) hypothetical liquid with absorbance of 0.1 m^{-1} . Computed amplitude noise limited DLs in ((e), (g), and (h)) water and (f) hypothetical liquid with SNR = 60 dB. Computed DLs in ((i), (k), and (l)) water and (j) hypothetical liquid with temperature noise and spectral noise. Computed DLs in ((m), (o), and (p)) water and (n) hypothetical liquid with temperature noise and spectral noise, assuming measurement up to 1% of the resonance linewidth.²⁰

hypothetical low-Q device, such as grating resonators, with $Q \sim 10^3$ and $f_B = 100\%$ (assuming $n_{\text{eff}} = 2.4$ and $n_g = 2$).

Since detection up to 1% of the linewidth is feasible,²² the numerator in Eq. (7) is multiplied by 0.01. At $Q_i = 1.6 \times 10^4$, $f_B = 10\%$, the calculated DL in silicon PC microcavity devices at 1550 nm with (and without) temperature and spectral noise is 5×10^{-7} RIU (2.5×10^{-8} RIU) at $n_g = 30$. Thus, at $n_g = 30$, a group index value achieved in PCWs,²³ the PC resonance sensors can exceed the ultimate DL of 1×10^{-7} in SPR systems.²⁴ The rise in n_g is accompanied by a decrease in Q to 8×10^3 , yet n_g dominates ultimate detection limits, since $Q_i > 5 \times 10^5$ in silicon are not useful due to various noises at 1550 nm.

In suitable designs of coupled PC microcavities¹⁹ with Q_i varying from 1×10^3 to 5×10^5 , if $f_B = 10\%$, calculated DL is nearly constant between 5.1×10^{-8} RIU and 5.8×10^{-8} RIU, with temperature and spectral noise. Under the same conditions, the ring resonator¹ is limited to 1×10^{-6} RIU at the maximum demonstrated slowdown factor of 16 in coupled rings.²⁵ One must consider a lower SNR at high n_g . If SNR = 10 dB, it would still enable DL of 2.3×10^{-7} RIU to 5.5×10^{-7} RIU in PCs at $n_g = 330$ for above f_B and range of Q_i .

For biosensing in water-based media, one may consider PC designs between 1200 and 1220 nm in silicon ($\alpha \sim 105 \text{ m}^{-1}$) or at 980 nm ($\alpha \sim 43 \text{ cm}^{-1}$) in GaAs due to lower water absorbance. At $n_g = 30$, DLs calculated are one order of magnitude lower at 1200 nm than at 1550 nm, considering temperature and spectral noise, and minimum measurable $\Delta\lambda$ equal to the resonance linewidth. At 1300 nm in Si, $\alpha \sim 715 \text{ m}^{-1}$, hence performance improvement will not be that significant over performance at 1550 nm. High Q silica and polymer ring resonators operating at $\lambda_m = 0.8 \mu\text{m}$ are limited to DLs greater than 1×10^{-6} RIU when measurement induced noises equal to those considered here are used in calculations.

Equation (1) assumes that $\Delta n/n$ is the same for all perturbed liquid regions. Equation (1) must be modified when analyzing monolayer binding in biosensing, since the RI change is restricted to the liquid-dielectric interface. f_i is the mode overlap integral in Eq. (2) taken over the available interfaces for biomolecule attachment.

The minimum detectable concentration (C_{min}) is dependent on Q , n_g , and f_i . From Ref. 13, the resonance wavelength shift ($\delta\lambda$) is proportional to the sensitivity (S) and biomolecule surface density (σ_p). From Eq. (9), $\delta\lambda$ can be expressed as¹³

$$\delta\lambda \propto \lambda \sigma_p \times f_i \times n_g. \quad (10)$$

C_{min} is proportional to the bulk DL and related inversely to f_i and n_g . Equation (10) does not account for the size of the detection area or affinity constant between a probe and its conjugate biomolecule.

Biosensing was conducted with biotin as probe receptor and avidin as target protein.¹⁰⁻¹² Fig. 4 plots $\delta\lambda$ versus concentration for 4 different PC microcavities, L13, L21, L55, and L13 with defect hole. When $R_D = 0.4 \times R$, the lowest concentration detected is 1 fM (67 fg/ml), compared to 10 pM in L13 cavity⁸ without defect holes.

The resonance mode frequency offset from the band edge is closest in L55 PC microcavity followed by L21 and

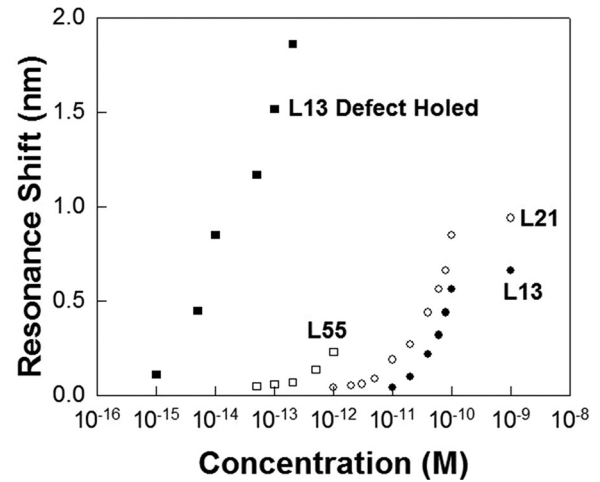


FIG. 4. Biosensing spectral shifts ($\delta\lambda$) in L13, L21, L55, and L13 defect holed PC microcavities.

L13. Since n_g increases with decreasing wavelength offset from the W1 PCW transmission band edge, a larger $\delta\lambda$ is observed in L55 with higher ($n_g \sim 20$) than in L21 ($n_g = 16$)¹² and L13 ($n_g = 13$) PC microcavities¹¹ for a given concentration as seen in Fig. 4. In addition to a larger optical mode volume, the larger $\delta\lambda$ in L55 PC microcavities, therefore, enhances the ability to detect lower concentrations, within the limitations set by measurement apparatus. Larger n_g in PC microcavities thus also results in larger $\delta\lambda$ and higher sensitivity when compared to ring resonators.

From Eq. (10), based on $n_g \sim 20$, the 22 μm long L55 PC microcavity is apparently 5 times more sensitive in biosensing than ring resonators. In the L55 PC microcavity, $\delta\lambda = 50 \text{ pm}$ at the minimum detected concentration of 3.35 pg/ml with avidin (67 kDa). The 30 μm diameter ring resonator detected a minimum 3.3 pg/ml of streptavidin (55 kDa); however, $\delta\lambda = 0.1 \text{ pm}$ (Ref. 1) which is 500 times smaller $\delta\lambda$ than the L55 PC microcavity, although binding affinities in both cases is same (dissociation constant $K_d \sim 10^{-15} \text{ M}$).²⁶ Furthermore, in Ref. 1, $\delta\lambda = 50 \text{ pm}$ is observed at 4×10^5 times higher concentration of 20 nM (1.1 $\mu\text{g/ml}$). The relation between $\delta\lambda$ and n_g in Eq. (10) is thus non-linear.

The larger f_i (due to larger f_B) for the L13 PC microcavity with defect holes results in a larger $\delta\lambda$ compared to the L13 PC microcavity without defect holes. Equation (10) and f_B data in Fig. 1(a) suggest a factor of 1.25 enhancement; however, experimental data show 4 orders of magnitude enhancement in minimum concentration detected in biosensing. Empirical data, therefore, suggest a superlinear relation between f_i and $\delta\lambda$ and hence the minimum experimentally detected concentration.

In summary, we showed that analyte absorbance, equipment limited spectral noise, and temperature noise, significantly contribute to the final achievable DL, irrespective of intrinsic Q and fill fractions. Slow light significantly enhances light-matter interaction and lowers the DLs. The benefits of slow light together with Q-factor and fill fraction were demonstrated in devices with moderate $Q \sim 10^4$. High sensitivity down to 67 fg/ml was experimentally demonstrated. Future designs can combine high n_g with high f_i and thus result in higher sensitivity in biosensing microarrays. Such a

combination of attributes is only potentially achievable currently on-chip in the photonic crystal platform.

This work was supported by the National Cancer Institute Contract No. HHSN261201200043C.

- ¹M. Iqbal, M. A. Gleeson, B. Spaugh, F. Tybor, W. G. Gunn, M. Hochberg, T. Baehr-Jones, R. C. Bailey, and L. C. Gunn, *IEEE J. Sel. Top. Quantum Electron.* **16**, 654 (2010).
- ²A. Densmore, M. Vachon, D. X. Xu, S. Janz, R. Ma, Y. H. Li, G. Lopinski, A. Delage, J. Lapointe, C. C. Luebbert, Q. Y. Liu, P. Cheben, and J. H. Schmid, *Opt. Lett.* **34**, 3598 (2009).
- ³H. Sipova, S. Zhang, A. M. Dudley, D. Galas, K. Wang, and J. Homola, *Anal. Chem.* **82**, 10110 (2010).
- ⁴M. Loncar, A. Scherer, and Y. M. Qiu, *Appl. Phys. Lett.* **82**(26), 4648–4650 (2003).
- ⁵D. Threm, Y. Nazirizadeh, and M. Gerken, *J. Biophoton.* **5**, 601 (2012).
- ⁶B. Zhang, A. Morales, R. Peterson, L. Tang, and J.-Y. Ye, *Biosens. Bioelectron.* **58C**, 107 (2014).
- ⁷S. Chakravarty, J. Topolancik, S. Chakrabarti, P. Bhattacharya, Y. Kang, and M. E. Meyerhoff, *Opt. Lett.* **30**, 2578 (2005).
- ⁸S. Zlatanovic, L. W. Mirkarimi, M. M. Sigalas, M. A. Bynum, E. Chow, K. M. Robotti, G. W. Burr, S. Esener, and A. Grot, *Sens. Actuators, B* **141**(1), 13–19 (2009).
- ⁹C. Kang, C. T. Phare, Y. A. Vlasov, S. Assefa, and S. M. Weiss, *Opt. Express* **18**, 27930–27937 (2010).
- ¹⁰S. Chakravarty, Y. Zou, W.-C. Lai, and R. T. Chen, *Biosens. Bioelectron.* **38**(1), 170–176 (2012).
- ¹¹W.-C. Lai, S. Chakravarty, Y. Zou, Y. Guo, and R. T. Chen, *Appl. Phys. Lett.* **102**, 041111 (2013).
- ¹²Y. Zou, S. Chakravarty, D. N. Kwong, W.-C. Lai, X. Xu, X. Lin, A. Hosseini, and R. T. Chen, *IEEE J. Sel. Top. Quantum Electron.* **20**(4), 6900710 (2014).
- ¹³I. M. White and X. Fan, *Opt. Express* **16**(2), 1020 (2008).
- ¹⁴N. A. Mortensen, S. Xiao, and J. Pedersen, *Microfluid. Nanofluid.* **4**, 117 (2008).
- ¹⁵K. K. Mehta, J. S. Orcutt, and R. J. Ram, *Appl. Phys. Lett.* **102**, 081109 (2013).
- ¹⁶E. Chow, A. Grot, L. W. Mirkarimi, M. M. Sigalas, and G. Girolami, *Opt. Lett.* **29**, 1093 (2004).
- ¹⁷W.-C. Lai, S. Chakravarty, X. Wang, C.-Y. Lin, and R. T. Chen, *Appl. Phys. Lett.* **98**, 023304 (2011).
- ¹⁸W. Bogaerts, P. De Heyn, T. Van Vaerenbergh, K. De Vos, S. K. Selvaraja, T. Claes, P. Dumon, P. Bientman, D. Van Thourhout, and R. Baets, *Laser Photon. Rev.* **6**(1), 47 (2012).
- ¹⁹J. Jagerska, N. Le Thomas, V. Zabelin, R. Houdre, W. Bogaerts, P. Dumon, and R. Baets, *Opt. Lett.* **34**(3), 359 (2009).
- ²⁰Y. Akahane, T. Asano, B.-S. Song, and S. Noda, *Nature* **425**, 944 (2003).
- ²¹K. De Vos, I. Bartolozzi, E. Schact, P. Bientman, and R. Baets, *Opt. Express* **15**(12), 7610 (2007).
- ²²F. Vollmer and S. Arnold, *Nat. Methods* **5**, 591 (2008).
- ²³X. Wang, C.-Y. Lin, S. Chakravarty, J. Luo, A. K.-Y. Jen, and R. T. Chen, *Opt. Lett.* **36**, 984 (2011).
- ²⁴M. Piliarik and J. Homola, *Opt. Express* **17**(19), 16505 (2009).
- ²⁵A. Canciamilla, M. Torregiani, C. Ferrari, F. Morichetti, R. M. De La Rue, A. Samarelli, M. Sorel, and A. Melloni, *J. Opt.* **12**, 104008 (2010).
- ²⁶R. J. McMahon, *Avidin-Biotin Interactions: Methods and Applications* (Humana Press, 2008).